Journal of Environmental Chemical Engineering 14 (2026) 124122

Contents lists available at ScienceDirect

Journal of Environmental Chemical Engineering

journal homepage: www.elsevier.com/locate/jece

Integrated room-temperature aqueous separation, purification, and regeneration of full-size commercial spent lithium-ion battery electrodes

Koji Abe [a,*], Yanko Marinov Todorov [a], Nobuaki Matsumoto [b], Yuko Sawaki [b]

[a] Organization for Research Initiatives, Yamaguchi University, 2-16-1 Tokiwadai, Ube, Yamaguchi 755-8611, Japan
[b] New Business Producing Division, Maxell, Ltd., 1 Koizumi, Oyamazaki, Oyamazaki-cho, Otokuni-gun, Kyoto 618-8525, Japan

ARTICLE INFO

Keywords:
Direct recycling
Aqueous recycling
Cathode delamination
Graphite regeneration
Residual lithium
Cycling history

ABSTRACT

This study investigates the aqueous separation, purification, regeneration, and electrochemical evaluation of cathode and anode materials recovered from commercial NCM523/graphite pouch cells cycled for 100–300 charge–discharge cycles and used after DMC rinsing without NaCl-solution discharge pretreatment. Under alkaline conditions (0.6–0.8 M NaOH) at ambient temperature, cathode active materials were spontaneously delaminated from Al current collectors without ultrasonication. Delamination occurred within a limited alkaline concentration range, where gas evolution accompanying Al dissolution may facilitate interfacial separation, although the delamination behavior was also influenced by alkaline conditions and alkali species. In contrast, immersion of cycled graphite anodes in water induced gas evolution associated with residual Li-containing species, promoting graphite detachment from Cu current collectors. Transition metals (Ni, Co, Mn, and Al) deposited on graphite during cycling were effectively removed by dilute H_2SO_4 treatment, and subsequent heat treatment restored electrochemical performance. The results demonstrate distinct aqueous separation behaviors for cathode and anode materials and suggest that preserving cycling-induced characteristics is important for understanding recycling-relevant phenomena in spent lithium-ion battery electrodes.

1. Introduction

In recent years, lithium-ion batteries (LIBs) have been increasingly deployed owing to the rapid expansion of electric vehicles and stationary energy storage systems, resulting in a growing volume of spent LIBs. Because spent LIBs contain valuable metals such as cobalt (Co), nickel (Ni), and lithium (Li), they are often regarded as an urban mine, and the development of environmentally sustainable recycling technologies has become increasingly important. LIB recycling technologies are generally classified into pyrometallurgical, hydrometallurgical, and direct recycling processes [1–4]. Among these approaches, direct recycling has attracted considerable attention because it enables recovery and reuse of both electrode active materials and metallic current collectors while reducing energy consumption and environmental impact. A key challenge in direct recycling is the separation of electrode materials from current collectors. Cathode sheets typically consist of layered oxide materials such as $LiCoO_2$ and NCM ($LiNi_xCo_yMn_zO_2$) coated on Al foil using polyvinylidene fluoride (PVDF) binders [4,5]. Various separation approaches, including thermal treatment, chemical processing, ultrasonication, mechanical agitation, and pulsed electrical discharge, have therefore been investigated [6–11]. Similarly, graphite-anode delamination from Cu foils has been investigated using ultrasonication, mechanical agitation, and selective separation approaches [12–17]. Recent review articles have comprehensively summarized electrode-material separation technologies and ultrasound-assisted recycling processes for spent LIBs [18,19].

However, most previous studies have focused primarily on electrode separation itself, often using small laboratory-scale specimens. The influence of cycling history on subsequent purification, regeneration, and electrochemical evaluation has been less systematically investigated. In addition, delamination behavior under room-temperature aqueous conditions without ultrasonication has received comparatively less attention. Although water-based CMC/SBR binder systems have largely replaced conventional PVDF binders in commercial LIBs because of their lower environmental impact, studies on the recycling behavior of cycled graphite anodes employing CMC/SBR binders remain relatively limited compared with those on cathode materials [20–22]. In practical recycling studies, spent LIBs with unknown service histories or subjected to NaCl discharge pretreatment prior to dismantling are commonly used [12,13]. Although effective for battery deactivation, prolonged

* Corresponding author.
E-mail address: abekoji@yamaguchi-u.ac.jp (K. Abe).

https://doi.org/10.1016/j.jece.2026.124122
Received 2 June 2026; Received in revised form 7 July 2026; Accepted 12 July 2026
Available online 13 July 2026

exposure to concentrated saline solutions may induce corrosion of current collectors, alter electrode/electrolyte interphases, and affect residual reactive lithium species and electrode surfaces [23].

Such effects are particularly relevant to direct recycling because they may influence subsequent regeneration and electrochemical performance [24,25].

In this study, commercial NCM523/graphite pouch cells (161 mm × 78 mm, 9.5 Ah) cycled for 100–300 charge–discharge cycles were dismantled without NaCl-solution discharge pretreatment. After DMC rinsing, cathode and anode sheets were recovered as intact full-size electrode sheets and subsequently tracked through separation, purification, regeneration, and electrochemical evaluation. Cathode delamination and graphite-anode separation were achieved under room-temperature aqueous conditions without ultrasonication, external electrical input, or high-temperature pretreatment.

Accordingly, this study focuses on three aspects relevant to direct recycling: (i) ultrasonic-free aqueous separation of cathode and anode electrodes at ambient temperature, (ii) cycling-history-dependent phenomena, including hydrogen evolution, residual lithium-containing species, transition-metal deposition, and graphite structural changes, and (iii) regeneration of recovered materials through purification and thermal treatment, followed by electrochemical evaluation.

2. Experimental

2.1. Chemical materials

Lithium carbonate (Li_2CO_3, >99%), lithium hydroxide monohydrate ($LiOH{\cdot}H_2O$, 98.0–102.0%), nitric acid (HNO_3, 60%), sulfuric acid (H_2SO_4, 95%), hydrochloric acid (HCl, 35–37%), and *N*-methyl−2-pyrrolidone (NMP, 99%) were purchased from FUJIFILM Wako Pure Chemical Corporation. Sodium hydroxide (NaOH, >99%) and potassium hydroxide (KOH, >85%) were purchased from Nacalai Tesque. Dimethyl carbonate (DMC, H_2O < 10 ppm) and an electrolyte consisting of 1 M $LiPF_6$ in ethylene carbonate/dimethyl carbonate (EC/DMC = 3/7, v/v) containing 1 wt% vinylene carbonate (VC) (H_2O < 10 ppm, HF < 30 ppm) were obtained from MU Ionic Solutions. A 5 wt% PVDF (#9305 KF) solution was obtained from Kureha Corporation.

2.2. Pouch cells

The cathode sheet consisted of $LiNi_{0.5}Co_{0.2}Mn_{0.3}O_2$ (NCM523) and polyvinylidene fluoride (PVDF) coated on both sides of an Al foil, while the anode sheet consisted of graphite, styrene–butadiene rubber (SBR), and carboxymethyl cellulose (CMC) coated on both sides of a Cu foil current collector.

Commercial NCM523/graphite pouch cells (161 mm × 78 mm, nominal capacity: 9.5 Ah, Maxell, Ltd.) were used in this study. Each cell contained 27 cathodes and 28 anodes stacked alternately, with each cathode enclosed in a separator pocket. The cathode and anode sheets accounted for approximately 45 and 35 wt% of the total cell mass, respectively, whereas the Al and Cu current collectors accounted for approximately 13 and 32 wt% of the cathode and anode sheet masses, respectively.

Charge–discharge cycling was performed at 25 °C using an ACD-M02C battery testing system (ASKA Electronic Co., Ltd.). The cells were charged in constant-current/constant-voltage (CC–CV) mode to 4.2 V and discharged to 2.7 V at 0.3 C based on the nominal capacity.

2.3. Electrolyte extraction and analysis

After discharge to 2.7 V at 0.3 C (3 A), the cells were transferred into an argon (Ar)-filled glove box to avoid moisture exposure. The cells were carefully opened to prevent short circuits, and the cell stack was immersed in 30 mL of DMC to extract the residual electrolyte. After 1 h, the stack was removed, sealed in a separate laminate bag, and taken out of the glove box. The recovered electrode sheets were subsequently used in their original dimensions without cutting.

A 10 mL aliquot of the electrolyte extract was concentrated at 60 °C under reduced pressure (5 kPa) using a rotary evaporator to remove volatile solvents. Concentrated HCl (2 mL) was then added, and the solution was diluted to 25 mL with deionized water. After filtration through a 0.2 μm membrane filter (DISMIC 25CS020AN, ADVANTEC), the sample was analyzed by inductively coupled plasma optical emission spectrometry (ICP–OES; SPS3500, Hitachi High-Tech).

2.4. Gas collection

Evolved gases were collected using a custom-made transparent polyvinyl chloride apparatus (Fig. 6a). Gas volumes were determined from the calibrated scale attached to the apparatus. The recovered cell stack was rapidly inserted into the lower part of the water-filled apparatus, and gas evolution was monitored for 30 min.

2.5. Cell disassembly and material separation

After immersion in water, the cell stack was separated into the cathode sheet, separator, and Cu foil. The graphite anode, which spontaneously detached from the Cu foil in water, was collected by filtration and dried in air at 60 °C overnight. The cathode sheet and separator were dried in air at room temperature overnight.

The cathode sheet was treated with 200 mL of alkaline or acidic aqueous solution to detach the active material from the Al foil. Alkaline treatment experiments were conducted in a SUS304 stainless-steel vessel, whereas acid treatment experiments were conducted in a polypropylene (PP) vessel. Ultrasonic treatment was performed for 10 min using an ultrasonic bath (ASU-3M, AS ONE Co., Japan; 42 kHz, 80 W). The recovered cathode active material was collected by filtration, washed with deionized water, and dried in air at 60 °C overnight. The Al foil was rinsed with deionized water and air-dried.

The filtrates from the alkaline and acidic treatments were analyzed by ICP–OES to evaluate the dissolution of Al from the current collector and Mn, Co, and Ni from the cathode active material.

2.6. ICP–OES analysis of deposited metals on the graphite anode

A 0.5 g sample of the graphite anode was immersed in 10 mL of concentrated HCl for 1.5 h. Deionized water (5 mL) was then added, and the mixture was filtered through a 0.2 μm membrane filter (DISMIC 25CS020AN, ADVANTEC). The filtrate was diluted to 50 mL with deionized water and analyzed by ICP–OES.

2.7. Regeneration methods

Recovered cathode powder (0.3–0.4 g) was dissolved in 10 mL of concentrated HCl under stirring, followed by heating at approximately 80 °C for 30 min. After cooling, the solution was diluted, filtered through a 0.2 μm membrane filter, further diluted 1000-fold, and analyzed by ICP–OES to determine the Li content. The Li deficiency of the recovered cathode material was estimated from the difference between the measured Li content and the stoichiometric lithium content of NCM523. Li_2CO_3 corresponding to the estimated Li deficiency was then added with an additional 3 mol% excess, following the procedure reported in Ref. [26], and mixed with the recovered cathode material by ball milling for 30 min. The mixture was calcined in air using a box furnace (KBF542N1, JTEKT Thermo Systems Co., Ltd.) and a high-purity alumina crucible (Al_2O_3 > 99.5%).

Recovered graphite anode material (approximately 20 g) was heat-treated under an Ar flow (1 L min^{-1}) using a bottom-loading muffle furnace equipped with a vacuum exchange system (SPS1216V, Marusho Electric Co., Ltd.).

2.8. Scanning electron microscopy (SEM) and X-ray diffraction (XRD)

The surface morphologies of the cathode and anode materials were observed using a scanning electron microscope (TM4000, Hitachi High-Tech). Cross-sectional images were obtained using a field-emission scanning electron microscope (S−4800, Hitachi High-Tech).

XRD patterns of regenerated cathodes were obtained using an Ultima IV X-ray diffractometer (Rigaku Corporation) with Cu Kα radiation operated at 40 kV and 30 mA at a scanning rate of 2° min^{-1} .

2.9. Charge–discharge evaluation

The regenerated cathode and anode materials were fabricated into single-sided electrodes using the same electrode formulation as the original pouch-cell electrodes. The electrodes were punched into 11 mm diameter disks, and coin cells with a nominal capacity of approximately 2 mAh were assembled using lithium metal as the counter electrode. Electrochemical measurements were conducted using a battery testing system (TOSCAT−3000, Toyo System Co., Ltd.).

For NCM523/Li half-cells, charge–discharge cycling was performed in constant-current/constant-voltage (CC–CV) mode. The cells were charged to 4.3 V at 0.1 C with a current cut-off of 0.02 C and discharged to 2.6 V at 0.1 C. Graphite/Li half-cells were tested at the same current rate between 0.01 and 3.0 V, where charge and discharge correspond to lithiation and delithiation of graphite, respectively.

2.10. Al–alkaline aqueous solution model experiments

A 50 mm × 50 mm Al foil (12 μm thick) or a PVDF-coated Al foil prepared by dipping the foil into a 1.2 wt% PVDF solution and drying at 80 °C for 30 min was placed in a flat Petri dish (inner diameter: 91 mm), and 30 mL of alkaline aqueous solution was added to observe gas evolution and Al dissolution behavior. To prevent the Al foil from floating owing to hydrogen evolution, a cross-shaped weight fabricated from 0.8 mm diameter SUS316 wire (Nilaco Corporation) was placed on the foil.

3. Results and discussion

3.1. Recycling process overview

Spent 9.5 Ah NCM523/graphite pouch cells cycled for 100–300 cycles were disassembled in an Ar atmosphere to minimize air exposure. After rinsing with dimethyl carbonate (DMC) to remove residual electrolyte, the recovered electrode assembly was immersed in water, where residual Li-containing species reacted with water accompanied by gas evolution, facilitating safe handling during subsequent processing.

After mechanical separation, the cathode and anode were treated independently. The cathode was immersed in aqueous NaOH, resulting in spontaneous delamination of the active material layer from the Al current collector without ultrasonication or mechanical agitation. The recovered cathode powder was filtered, dried, mixed with Li_2CO_3, and calcined to restore electrochemical performance.

The anode was treated with dilute H_2SO_4 to remove deposited metallic species, followed by thermal regeneration. The overall process enabled aqueous-based separation, purification, and regeneration of both electrodes under ambient conditions (Fig. 1).

3.2. Aqueous alkaline treatment

The cathode sheet was immersed in 0.7 M NaOH aqueous solution, where gas evolution was observed at the cathode/Al interface (Fig. 2a). Spontaneous delamination of the active material layer from the Al foil occurred within approximately 5 min without ultrasonication. Delamination was evaluated by visual inspection and the presence of residual active material on the Al surface.

The simultaneous occurrence of gas evolution and interfacial separation suggests that gas generation accompanying Al dissolution may contribute to disruption of the cathode/Al interface. However, the amount of evolved gas was substantially smaller than that quantified for spent graphite anodes (Section 3.7). Therefore, the relative contributions of gas evolution, Al dissolution, and other interfacial processes could not be distinguished quantitatively.

Delamination behavior depended on alkali concentration and species. In 0.6 M NaOH, incomplete delamination was observed, whereas 0.8 M NaOH promoted efficient delamination but caused partial

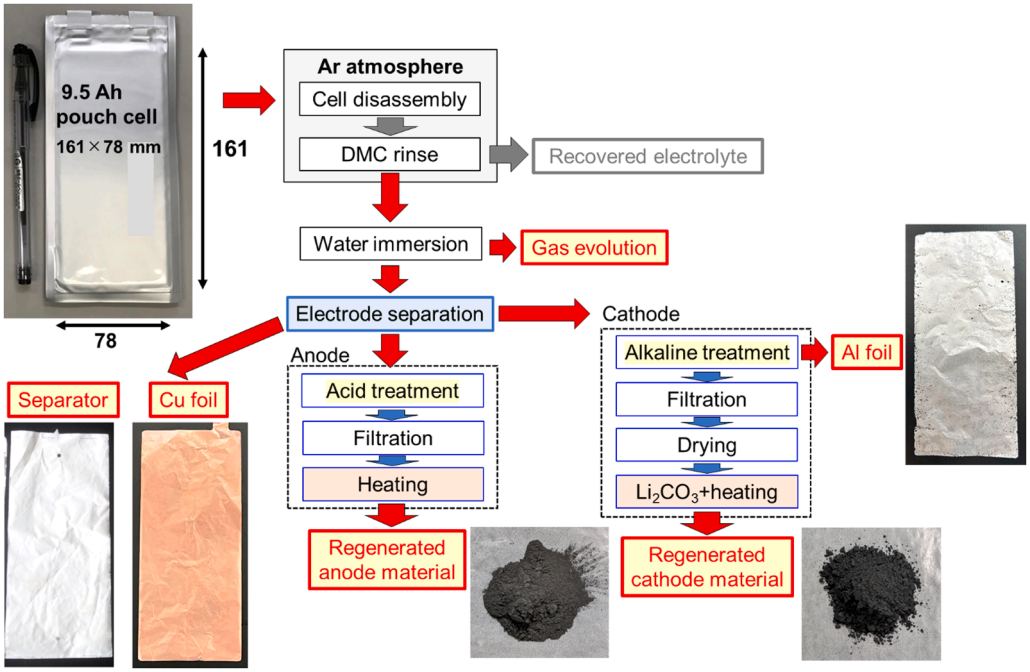

Fig. 1. Flow diagram of the aqueous recycling process for spent LIB electrodes.

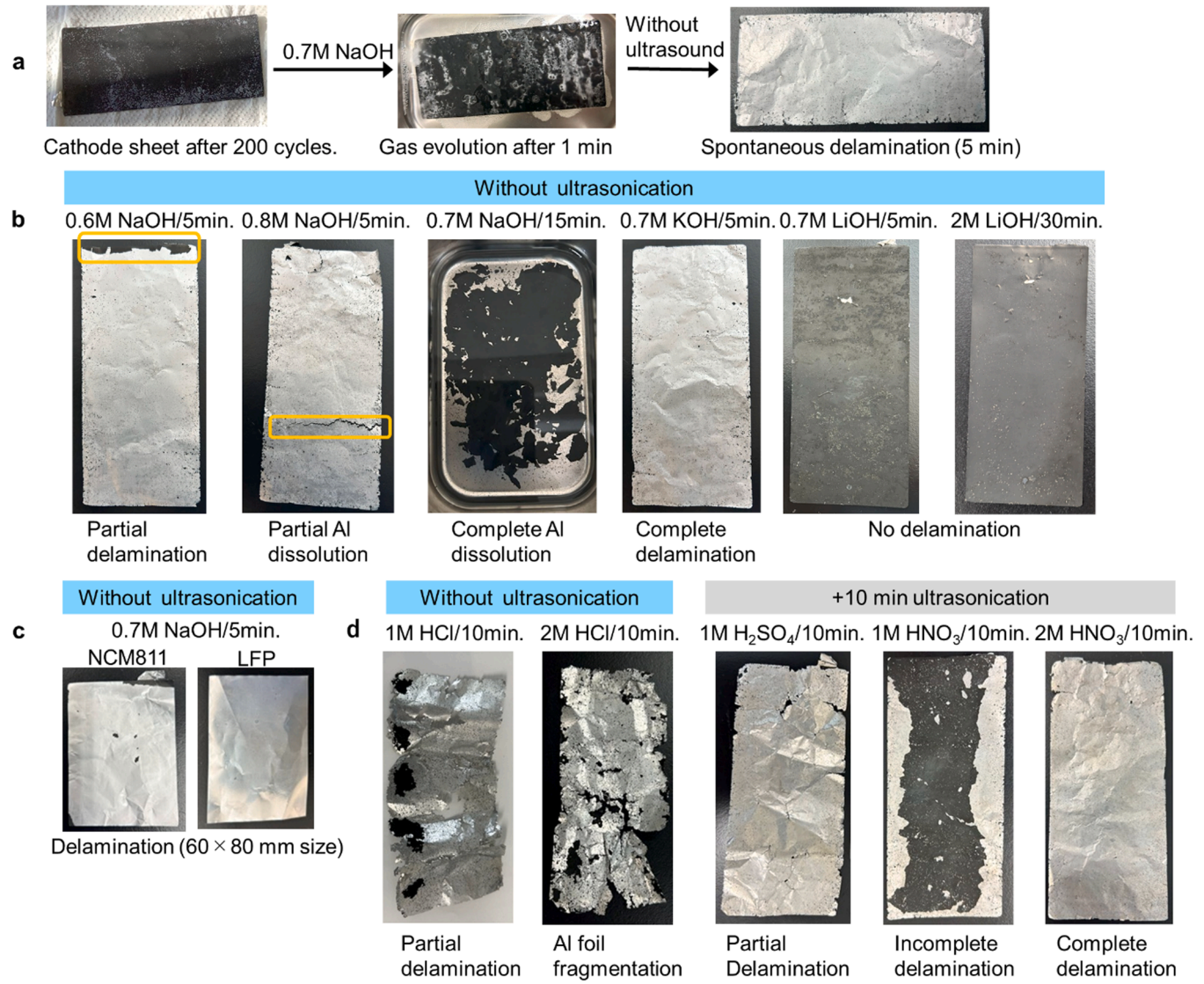

Fig. 2. Photographs showing the delamination behavior of cathode sheets in alkaline aqueous solutions (a–c) and an inorganic acid aqueous solution (d).

dissolution of the Al foil. Under 0.7 M NaOH, complete dissolution of the Al foil occurred after 15 min, indicating that prolonged exposure degrades the current collector. No delamination was observed in 0.7 M or 2.0 M LiOH, whereas 0.7 M KOH showed behavior comparable to that in NaOH (Fig. 2b).

To further examine the delamination mechanism, bare Al foil and PVDF-coated Al foil were immersed in 0.7 M NaOH, 0.7 M LiOH, and 2.0 M LiOH solutions (Fig. S1). For bare Al foil, gas evolution was more vigorous and uniformly distributed in 0.7 M NaOH and 2.0 M LiOH than in 0.7 M LiOH (Fig. S1a). Complete dissolution occurred within approximately 10 min in 0.7 M NaOH, 13 min in 2.0 M LiOH, and 15 min in 0.7 M LiOH.

In contrast, gas evolution from PVDF-coated Al foil was substantially suppressed in all solutions, and differences in bubble morphology and distribution became less apparent. The commercial NCM523 cathode sheet (Fig. 2a) exhibited weak gas evolution comparable to that observed for the PVDF-coated Al foil. After 30 min of immersion, the PVDF-coated Al foil completely disappeared in 0.7 M NaOH, whereas it remained largely intact in 2.0 M LiOH and retained its original shape in 0.7 M LiOH (Fig. S1b).

These observations suggest that the PVDF coating partially limits contact between the alkaline solution and Al, thereby suppressing Al dissolution. Although gas evolution may facilitate interfacial separation, alkalinity and gas evolution alone do not fully explain the delamination behavior. Notably, spontaneous delamination was not observed even in 2.0 M LiOH despite rapid dissolution of bare Al foil. The present results therefore suggest that delamination of PVDF-containing electrodes is influenced by both gas-assisted interfacial separation and suppression of Al dissolution by the PVDF coating.

Overall, delamination depended on alkaline concentration, immersion time, and alkali species. Under the conditions investigated, 0.7 M NaOH provided a practical operating range that enabled efficient delamination while minimizing excessive Al dissolution. Further confirmation of the evolved gas composition by direct gas analysis will be required to clarify its role in the delamination process.

Preliminary experiments using 80 mm × 60 mm NCM811 and $LiFePO_4$ cathode sheets showed qualitatively similar behavior (Fig. 2c). However, these experiments were intended only to confirm feasibility, and detailed investigation is beyond the scope of the present study.

3.3. *Inorganic acid aqueous treatment*

When the cathode sheet was immersed in 1 M HCl, partial delamination of the active material layer occurred without ultrasonication. Delamination also occurred in 2 M HCl; however, severe corrosion of the Al foil was simultaneously observed. In contrast, 1 M H_2SO_4 and 1–2 M

HNO_3 failed to induce delamination under static conditions, and only partial separation was achieved even after ultrasonication (Fig. 2d). Thus, HCl promoted delamination but caused substantial Al dissolution, whereas H_2SO_4 and HNO_3 showed limited delamination efficiency and generally required ultrasonic assistance.

Overall, under the investigated conditions, inorganic acids were less suitable for cathode separation than alkaline solutions because they either caused severe Al corrosion or required ultrasonication for effective delamination.

3.4. Summary of separation and purification behavior of cathode sheets

Fig. 3 summarizes the cathode delamination behavior under the investigated conditions. Delamination without mechanical assistance was observed only within a limited alkaline concentration range (0.6–0.8 M NaOH), whereas incomplete separation or excessive Al dissolution occurred outside this range.

Spontaneous delamination without ultrasonication was achieved in 0.7 M NaOH, 0.7 M KOH, and 1 M HCl. Among these conditions, 0.7 M NaOH exhibited the lowest transition-metal dissolution (0.04%) while maintaining relatively low Al dissolution, whereas the corresponding transition-metal loss in 0.7 M KOH was slightly higher (0.06%) (Fig. 3a). Although HCl also enabled spontaneous delamination, acidic media promoted greater transition-metal dissolution than alkaline media (Fig. 3a), consistent with previous reports that NCM523 undergoes transition-metal dissolution under strongly acidic conditions, particularly below pH 2 [27].

Fig. 3b schematically summarizes the delamination behavior observed in this study. Under alkaline conditions, gas evolution accompanying Al dissolution may facilitate interfacial separation, whereas excessive alkalinity accelerates Al dissolution and insufficient reactivity results in incomplete separation. In contrast, acidic media generally provided less favorable conditions for cathode recovery because of either severe Al corrosion (HCl) or limited delamination efficiency (H_2SO_4 and HNO_3).

Overall, these results suggest that 0.7 M NaOH provides a practical operating range for spontaneous delamination of large-area cathode sheets under ambient aqueous conditions without ultrasonication. Although treatment of the resulting alkaline waste solution was beyond the scope of this study, precipitation-based treatment of such alkaline recycling solutions has been reported previously [28].

a

Aqueous	M	Ultrasound	NCM loss (%)	Al foil loss (%)
NaOH	0.7	Unnecessary	0.04	6.8
KOH	0.7		0.06	17.7
HCl	1		10.1	11.3
H_2SO_4	1	Necessary	1.3	3.2
HNO_3	2		4.0	9.9

b

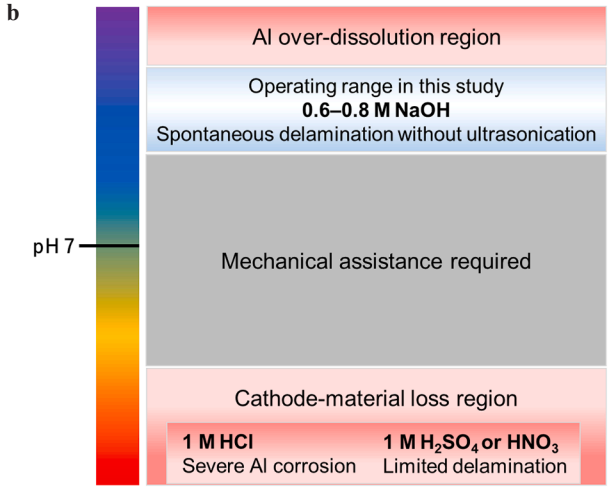

Fig. 3. (a) Dissolution ratios of Ni, Co, Mn, and Al under different treatment conditions. (b) Summary of cathode delamination behavior under different treatment conditions.

3.5. Calcination conditions for recovered cathode materials

The electrochemical performance of the recovered cathode material strongly depended on the calcination conditions (Fig. 4). The as-recovered (non-calcined) sample exhibited a low initial discharge capacity of 17 mAh g^{-1} with a coulombic efficiency of 59%, which may be associated with residual binder, Li deficiency, and cycling-induced degradation.

Calcination at 600 °C increased the discharge capacity to 103 mAh g^{-1} , while the addition of Li_2CO_3 further improved the capacity to 122 mAh g^{-1} , indicating that Li supplementation contributes to electrochemical recovery. Subsequent calcination at 900 °C increased the discharge capacity to 144 mAh g^{-1} with a coulombic efficiency of 81% in a covered crucible. Calcination in an open crucible further improved the performance to 151 mAh g^{-1} with a coulombic efficiency of 85%, suggesting that subtle differences in the thermal environment influence regeneration behavior even under nominally identical atmospheric conditions.

The improved performance at higher calcination temperatures is consistent with previous studies on regenerated layered NCM materials, where high-temperature calcination enhances structural ordering and electrochemical properties [29]. The discharge capacity obtained in this study is comparable to previously reported values for regenerated NCM523 cathodes [30], indicating that the proposed aqueous recycling process can restore the electrochemical performance of spent NCM523 cathodes to a comparable level. Optimization of the calcination conditions was beyond the scope of the present study.

3.6. SEM and XRD characterization of recovered cathode materials

Cross-sectional SEM images of the cathode materials are shown in Fig. 5, and X-ray diffraction patterns of Li_2CO_3-added cathodes heat-treated at various temperatures are shown in Fig. 6.

In the as-recovered (non-calcined) sample, features attributable to residual conductive additives and PVDF binder were observed in the cross-sectional SEM image, suggesting that the active-material particles were not fully exposed (Fig. 5a). After heat treatment at 600 °C for 5 h, the active-material particles appeared to be more clearly exposed in the cross-sectional SEM image (Fig. 5b). This morphological change is consistent with thermal decomposition of PVDF reported to occur at approximately 500 °C [31], although the complete removal of binder-derived species could not be confirmed in the present study.

Cross-sectional SEM observations of the 600 °C-treated sample revealed microcracks within secondary particles (Fig. 5b), possibly associated with thermally induced stresses during heat treatment. Similar microcracks have been reported for layered NCM materials [32]. In contrast, the sample subjected to the two-step treatment (600 °C for 5 h followed by 900 °C for 15 h) with Li_2CO_3 addition showed no obvious crack formation in the observed region (Fig. 5c), consistent with the improved electrochemical performance discussed in Section 3.5.

To evaluate possible structural changes induced by alkaline treatment, XRD patterns of the recovered cathode material before and after NaOH treatment were examined. No additional diffraction peaks, peak splitting, or significant peak shifts were observed after NaOH treatment (Fig. S2), suggesting that no appreciable changes occurred in the layered NCM523 framework under the present treatment conditions. Furthermore, ICP–OES analysis showed only minor increases in Al (<0.1 wt%)

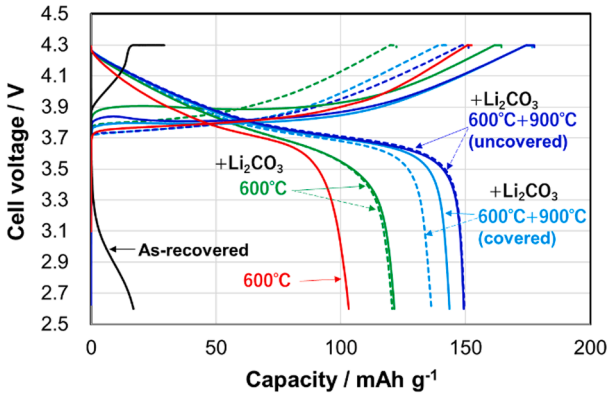

1M $LiPF_6$ [EC/DMC=3/7(v/v)]+1wt%VC
Charge: 4.3V 0.1C CC-CV 0.02C cut
Discharge: 0.1C 2.6V cut

Calcination in air 600℃, 5h; 900℃, 15h	1st (2nd) charge / mAh g^{-1}	1st (2nd) discharge / mAh g^{-1}	1st (2nd) CE / %
As-recovered	29	17	58
600℃	153	103	68
+Li_2CO_3 600℃	165 (122)	122 (121)	74 (99)
+Li_2CO_3 600℃+900℃ (covered crucible)	177 (142)	144 (136)	81 (96)
+Li_2CO_3 600℃+900℃ (uncovered crucible)	178 (151)	149 (150)	84 (99)

Fig. 4. Charge–discharge curves of recovered cathode materials under different calcination conditions. Solid line: 1st cycle; dashed line: 2nd cycle.

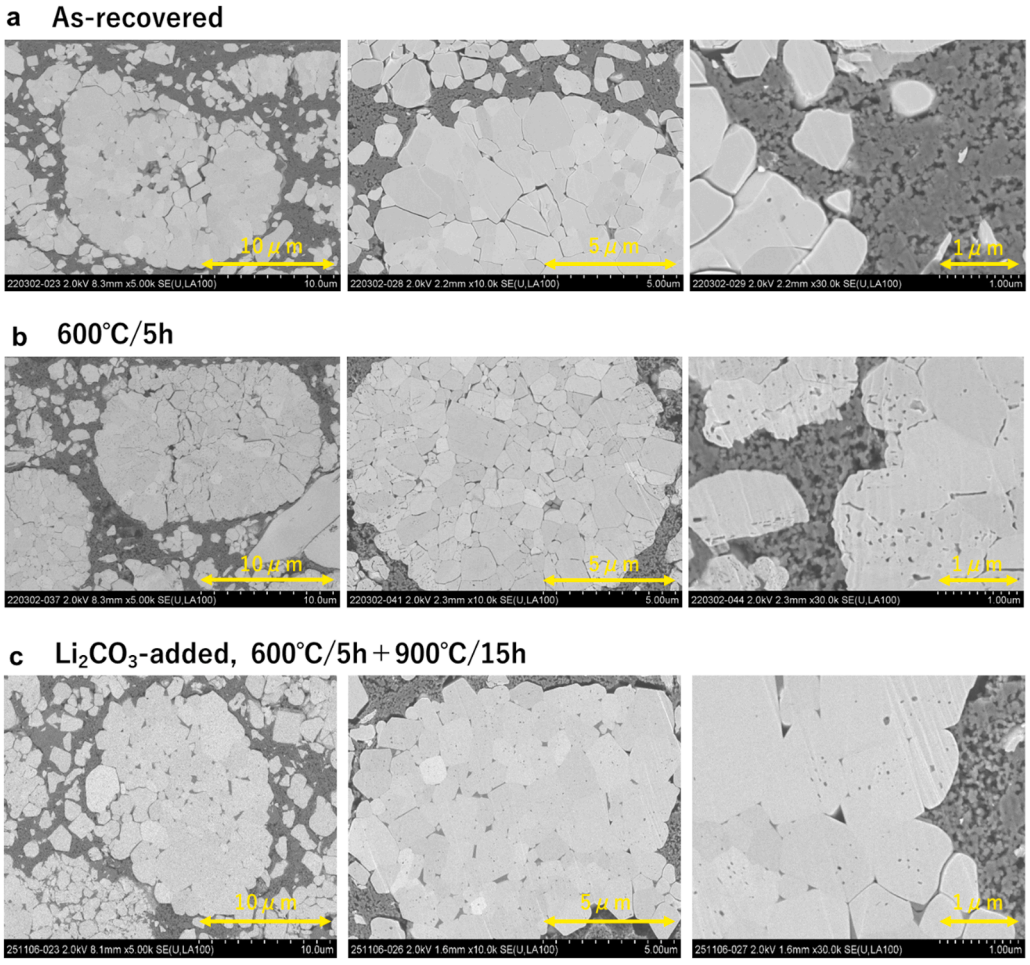

Fig. 5. Cross-sectional SEM images of cathode materials after different regeneration treatments.

and Na (<0.03 wt%) contents after alkaline treatment, indicating limited contamination of the recovered cathode material under the present conditions.

Overall, the SEM and XRD results suggest that the proposed process removes residual organic species while preserving the layered structure of the cathode material, which is consistent with the electrochemical recovery behavior discussed in Section 3.5.

3.7. H_2 evolution in anode and estimation of residual Li

In this study, gas evolution was observed when the mixed cathode/anode electrode assembly obtained after pouch-cell disassembly and DMC rinsing was immersed in water (Fig. 7). No gas evolution was visually observed from the cathode side, suggesting that the reaction originated primarily from residual Li-containing species remaining in the graphite anode.

Particularly vigorous gas evolution was observed during the first 5–10 min after immersion of graphite electrodes recovered from cycled pouch cells, with a continuous stream of bubbles emitted from the electrode surface. The gas evolution was readily visible over the entire electrode surface, decreased rapidly thereafter, and became negligible after approximately 30 min of immersion. Exposure of the evolved gas to

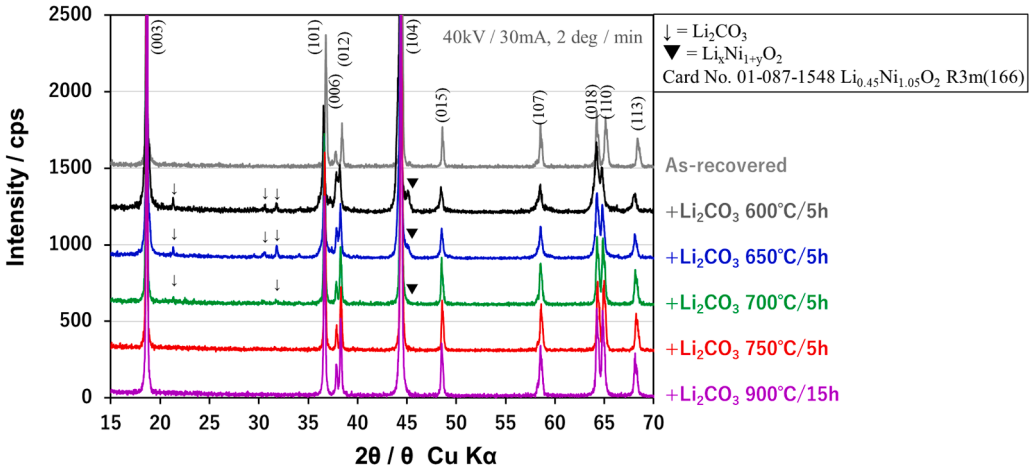

Fig. 6. X-ray diffraction patterns of Li_2CO_3-added cathodes heat-treated at various temperatures.

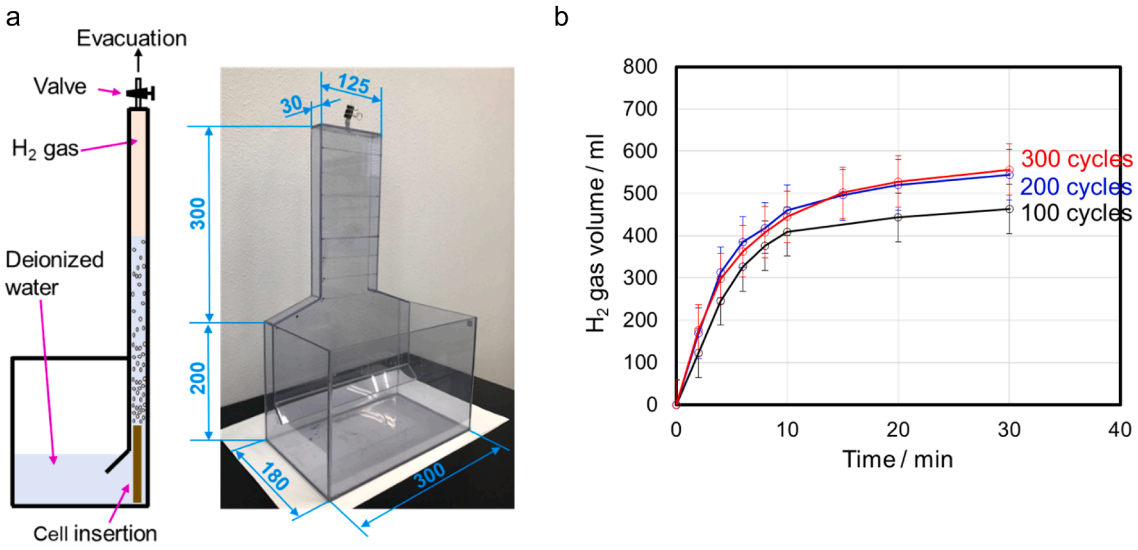

Fig. 7. (a) Experimental setup for gas collection. (b) Time-dependent gas evolution during water immersion.

a flame resulted in brief ignition accompanied by a "pop" sound, indicating the presence of H_2. However, the gas composition was not directly analyzed in the present study. The inference that H_2 was the dominant component is based on the ignition behavior and the known reaction of lithiated graphite species with water.

Similar hydrogen evolution during water treatment of spent graphite anodes has been reported previously for PVDF-based graphite electrodes, where H_2 evolution was suggested to facilitate removal of the solid electrolyte interphase (SEI) from graphite surfaces [33]. However, to the best of our knowledge, no previous study has directly identified hydrogen evolution associated with the spontaneous detachment of cycled commercial CMC/SBR graphite anodes from Cu foil during water immersion.

The total volume of evolved gas increased with cycle number (100 cycles: 460 cm^3, 200 cycles: 540 cm^3, and 300 cycles: 560 cm^3), suggesting that the amount of reactive residual Li-containing species in the graphite anode increased with cycling. The vigorous gas evolution observed mainly within the first approximately 10 min after immersion coincided with the detachment of graphite particles from the Cu current collector.

A rough estimation based on the evolved gas volume from the electrode after 300 cycles and discharge to 2.7 V suggests that approximately 0.053 mol of reactive Li-containing species remained available for reaction with water in a 10 Ah-class electrode, corresponding to approximately 14% of the theoretical Li inventory (0.373 mol Li per cell). Because the chemical nature of the residual Li species was not identified, this value should be regarded as a semi-quantitative estimate.

Gas evolution may facilitate detachment of graphite particles during water immersion, and its volume may serve as a qualitative indicator of residual reactive Li-containing species in spent graphite anodes. No gas evolution was observed for fresh graphite electrodes, whereas gas evolution became increasingly pronounced with cycle number. These observations suggest that the recycling behavior of spent graphite anodes differs from that of fresh electrodes and should be considered in recycling-process evaluation.

3.8. *Metal deposition on anode/electrolyte and acid removal*

The amounts of deposited metal species (Ni, Co, Mn, and Al) on graphite anodes and in the electrolyte were quantified as a function of cycle number (Figs. 8a and 8b). The total amount of metal species detected on the graphite surface was approximately one order of magnitude higher than that remaining in the electrolyte (Fig. 8c), suggesting that transition-metal species released during cycling were deposited on the graphite surface to a much greater extent than they remained in the electrolyte, consistent with previous reports [26].

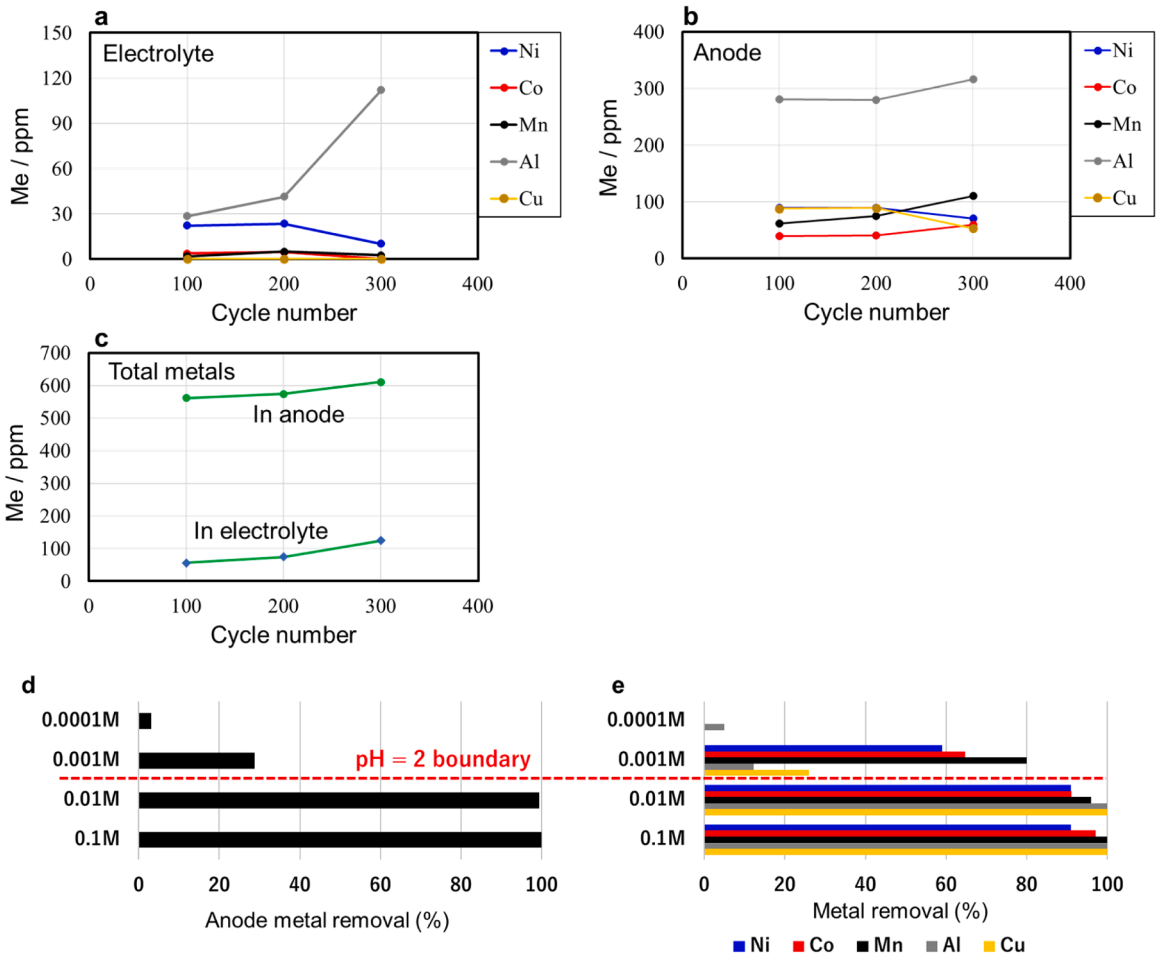

Fig. 8. ICP analysis of metal species (Ni, Co, Mn, and Al) present in the (a) electrolyte and (b) graphite anode, and (c) comparison of their distributions. (d, e) Effect of H_2SO_4 concentration on metal removal efficiency from the graphite anode.

To remove these deposited species, acid treatment was investigated. H_2SO_4 concentrations of 0.01 M or higher achieved removal efficiencies exceeding 90% for Ni, Co, and Mn (Figs. 8d and 8e), whereas lower concentrations were considerably less effective. Additional experiments using HCl and HNO_3 showed that HCl exhibited comparable removal performance to H_2SO_4, whereas HNO_3 was less effective. Considering both removal efficiency and handling safety, H_2SO_4 was selected for subsequent purification experiments.

Overall, these results demonstrate that transition-metal species accumulated on graphite surfaces during cycling can be effectively removed by dilute H_2SO_4 treatment, indicating that acid washing is a useful purification step prior to regeneration of spent graphite anodes.

3.9. Thermal treatment and electrochemical properties of recovered graphite anodes

The electrochemical performance of the recovered graphite anode strongly depended on the heat-treatment conditions, demonstrating the

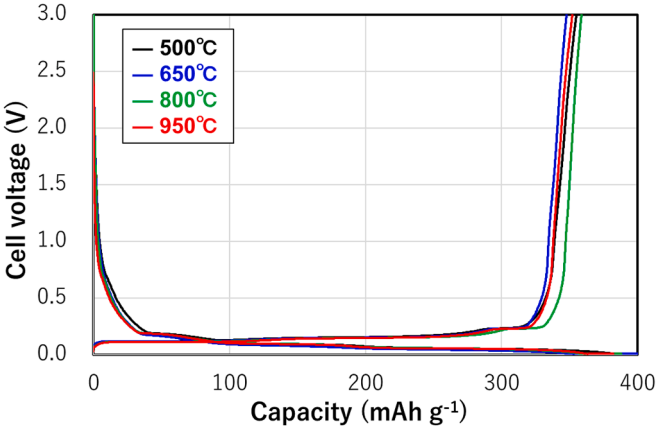

1M $LiPF_6$ [EC/DMC=3/7(v/v)]＋1wt%VC
Charge：0.01V 0.1C CC-CV 0.02C cut
Discharge：0.1C 3V cut

Heat treatment under Ar for 5 h	1st lith. / mAh g-1	1st delith. / mAh g-1	1st CE / %
500℃	417	355	85
650℃	403	348	86
800℃	388	359	92
950℃	383	352	92

Fig. 9. Charge–discharge curves of recovered graphite anodes under different thermal treatment conditions.

importance of thermal processing for performance recovery (Fig. 9).

For the sample treated at 500 °C for 5 h under an Ar atmosphere, the initial charge and discharge capacities were 417 and 355 mAh g^{-1}, respectively, with a coulombic efficiency of 85%. The apparent charge capacity exceeding the theoretical capacity of graphite (372 mAh g^{-1}) is likely associated with irreversible side reactions and decomposition of residual binder-derived species, such as SBR and CMC, remaining on the graphite surface. CMC/SBR binders are known to undergo multi-step thermal decomposition, with residual decomposition processes occurring between approximately 450 and 600 °C [34]. An Ar atmosphere was employed to suppress oxidation of graphite during heat treatment.

Increasing the treatment temperature gradually improved the electrochemical performance. At 650 °C for 5 h, the charge/discharge capacities were 403/348 mAh g^{-1} with a coulombic efficiency of 86%. At 800 °C, the capacities reached 388/359 mAh g^{-1} with a coulombic efficiency of 92%, whereas no further improvement was observed at 950 °C (383/352 mAh g^{-1}, 92%). These results suggest that heat treatment at approximately 800 °C is sufficient to recover most of the electrochemical performance of spent graphite under the present conditions. This tendency is consistent with previous reports showing that heat treatment reduces impurity content and improves the electrochemical properties of recycled graphite [22].

Thermal processing of graphite materials has been widely investigated. Synthetic graphite typically requires carbonization at around 1000 °C followed by graphitization at 2000–2800 °C under inert atmospheres [35], reflecting the high energy demand of its production process. In contrast, natural graphite generally requires only moderate heat treatment around 1000 °C for impurity removal and defect reduction [36]. Since natural graphite is widely used in commercial automotive LIB anodes, the present results suggest that regeneration of spent graphite can be achieved by moderate-temperature heat treatment without the high-temperature graphitization step required for synthetic graphite production, potentially reducing energy demand.

3.10. Cross-sectional structure of recycled graphite and residual Li

SEM observations of the regenerated graphite after heat treatment showed no significant morphological changes at the individual particle level (Figs. 10a and 10b). However, cross-sectional images of the electrode sheet exhibited slightly larger interparticle voids than those in the fresh electrode (Figs. 10c and 10d), which may be associated with structural changes induced by repeated Li intercalation and deintercalation during cycling.

Despite water immersion for Cu foil detachment and subsequent H_2SO_4 treatment for removal of deposited metals, the residual Li content in the recovered graphite was 563 ppm, substantially higher than that in the fresh graphite anode (0.55 ppm). This amount corresponds to approximately 2.2 mAh g^{-1}, equivalent to about 0.6% of the theoretical capacity of graphite. The chemical state of the residual Li species could not be identified in the present study.

The persistence of residual Li after separation and purification indicates that a fraction of cycling-derived Li-containing species remained in the recovered graphite despite water immersion and acid washing. Such residual Li was not detected in fresh graphite and may therefore be characteristic of graphite recovered from cycled cells. This observation is consistent with the H_2 evolution behavior discussed in Section 3.7 and suggests that spent graphite anodes exhibit recycling-relevant properties distinct from those of unused graphite materials.

3.11. Effects of cycling history on recycling behavior

Complete delamination of fresh graphite anodes has been reported to require mechanical treatment, such as ultrasonication or agitation [37]. In the present study, fresh graphite anodes did not exhibit gas evolution during water immersion, whereas cycled graphite anodes generated gas bubbles that promoted spontaneous detachment from the Cu current collector. Consequently, graphite separation, Cu foil recovery, removal of deposited metal species, and restoration of electrochemical performance were achieved without mechanical treatment.

Gas evolution, transition-metal deposition, interparticle void formation, and residual Li observed in cycled graphite anodes indicate that battery aging influences recycling behavior. These features are generally absent in fresh electrodes and may be altered or removed by conventional NaCl-solution pretreatment. They could therefore be examined using electrodes recovered with minimal pretreatment.

Importantly, the same batch of recovered materials was tracked through separation, purification, regeneration, and electrochemical evaluation, providing insight into interconnected processes relevant to practical direct recycling of LIBs that may be difficult to obtain using fresh or extensively pretreated electrodes.

4. Conclusion

This study demonstrated an aqueous direct recycling process for spent NCM523/graphite pouch-cell electrodes. Spontaneous cathode delamination was achieved within a limited alkaline concentration range at ambient temperature without ultrasonication or intensive mechanical treatment. The recovered cathode material was regenerated by Li_2CO_3 addition and calcination, restoring electrochemical performance to a level comparable with previously reported regenerated NCM523 materials [38].

For cycled graphite anodes, water immersion induced gas evolution

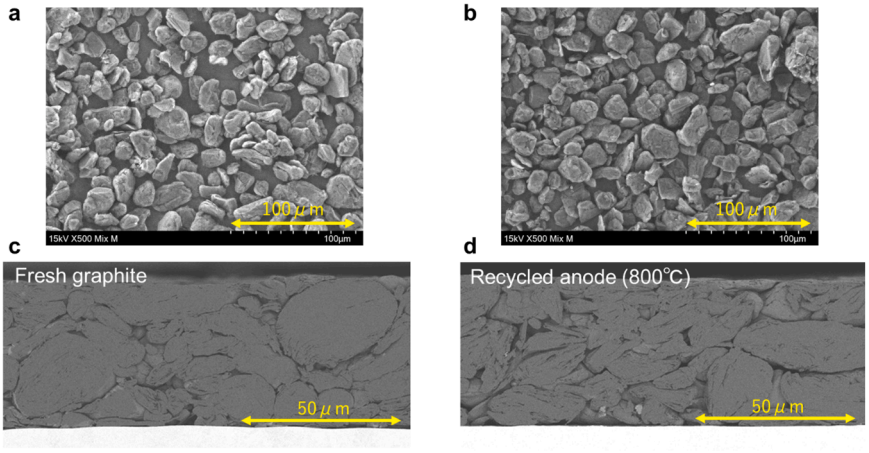

Fig. 10. Surface and cross-sectional SEM images of fresh (a and c) and recycled (b and d) graphite anodes.

associated with residual Li-containing species, facilitating graphite detachment from the Cu current collector. Deposited transition-metal species were effectively removed by dilute H_2SO_4 treatment, and subsequent heat treatment restored the electrochemical performance of the recovered graphite.

The electrodes were recovered without NaCl-solution discharge pretreatment, enabling separation, purification, regeneration, and electrochemical evaluation using the same batch of recovered materials. This approach revealed recycling-relevant phenomena associated with battery aging, including gas evolution, transition-metal deposition, and residual Li-containing species. These findings highlight the importance of preserving cycling-induced characteristics when assessing direct recycling processes for spent LIBs.

CRediT authorship contribution statement

Nobuaki Matsumoto: Visualization, Validation, Methodology, Investigation, Formal analysis, Data curation. **Yuko Sawaki:** Visualization, Validation, Methodology, Investigation, Formal analysis, Data curation, Conceptualization. **Koji ABE:** Writing – review & editing, Writing – original draft, Supervision, Resources, Methodology, Investigation, Funding acquisition, Data curation, Conceptualization. **Todorov Yanko:** Writing – review & editing, Visualization, Validation, Methodology, Investigation, Formal analysis, Data curation, Conceptualization.

Declaration of Competing Interest

The authors declare that they have no known competing financial interests or personal relationships that could have appeared to influence the work reported in this paper.

Appendix A. Supporting information

Supplementary data associated with this article can be found in the online version at doi:10.1016/j.jece.2026.124122.

Data availability

Data will be made available on request.

References

[1] S. Doose, J.K. Mayer, P. Michalowski, A. Kwade, Metals 11 (2021) 291, https://doi.org/10.3390/met11020291.
[2] K. Du, E.H. Ang, X. Wu, Y. Liu, Energy Environ. Mater. 5 (2022) 1012, https://doi.org/10.1002/eem2.12271.
[3] A. Zanoletti, E. Carena, C. Ferrara, E. Bontempi, Batteries 10 (2024) 38, https://doi.org/10.3390/batteries10010038.
[4] H. Shi, J. Zhang, L. Ou, Sep. Purif. Technol. 360 (2025) 130847, https://doi.org/10.1016/j.seppur.2024.130847.
[5] K. Abe, H. Yoshitake, T. Kitakura, T. Hattori, H. Wang, M. Yoshio, Electrochim. Acta 49 (2004) 4613, https://doi.org/10.1016/j.electacta.2004.05.016.
[6] L.P. He, S.Y. Sun, X.F. Song, J.G. Yu, Waste Manag. 46 (2015) 523, https://doi.org/10.1016/j.wasman.2015.08.035.
[7] F. Forte, M. Pietrantonio, S. Pucciarmati, M. Puzone, D. Fontana, Crit. Rev. Environ. Sci. Technol. 51 (2020) 2232, https://doi.org/10.1080/10643389.2020.1776053.
[8] H. Gao, Q. Yan, P. Xu, H. Liu, M. Li, P. Liu, J. Luo, Z. Chen, ACS Appl. Mater. Interfaces 12 (2020) 51546, https://doi.org/10.1021/acsami.0c15704.
[9] C. Lei, I. Aldous, J.M. Hartley, D.L. Thompson, S. Scott, R. Hanson, P.A. Anderson, E. Kendrick, R. Sommerville, K.S. Ryder, A.P. Abbott, Green. Chem. 13 (2021) 4710, https://doi.org/10.1039/D1GC01623G.
[10] Y. Yamada, Y. Kondo, H. Kondo, Waste Manag. 204 (2025) 114969, https://doi.org/10.1016/j.wasman.2025.114969.
[11] C. Tokoro, S. Lim, K. Teruya, M. Kondo, K. Mochidzuki, T. Namihira, Y. Kikuchi, Waste Manag. 125 (2021) 15, https://doi.org/10.1016/j.wasman.2021.01.008.
[12] X. Ren, Z. Tong, Y. Dai, G. Ma, Z. Lv, X. Bu, M. Bilal, A.B. Vakylabad, A. Hassanzadeh, Separations 10 (4) (2023) 246, https://doi.org/10.3390/separations10040246.
[13] W. Yang, Z. Tong, X. Bu, L. Dong, S.C. Chelgani, ACS Omega 10 (2025) 11214, https://doi.org/10.1021/acsomega.4c10547.
[14] S. Natarajan, V. Aravindan, Adv. Energy Mater. 10 (2020) 2002238, https://doi.org/10.1002/aenm.202002238.
[15] S. Natarajan, M.L. Divya, V. Aravindan, J. Energy Chem. 71 (2022) 351, https://doi.org/10.1016/j.jechem.2022.04.012.
[16] Y. Bai, M. Li, C.J. Jafta, Q. Dai, R. Essehli, B.J. Polzin, I. Belharouak, Sustain. Mater. Technol. 35 (2023) e00542, https://doi.org/10.1016/j.susmat.2022.e00542.
[17] Y. Kong, Y. Takaya, M. Cordova-Udaeta, C. Tokoro, Waste Manag. 188 (2024) 60, https://doi.org/10.1016/j.wasman.2024.07.033.
[18] W. Yang, Z. Tong, X. Bu, L. Dong, J. Ind. Eng. Chem. 148 (2025) 27, https://doi.org/10.1016/j.jiec.2024.12.074.
[19] Z. Tong, X. Ren, M. Ni, X. Bu, L. Dong, Energy & Fuels 37 (2023) 1474, https://doi.org/10.1021/acs.energyfuels.3c02290.
[20] J.-H. Lee, U. Paik, V.A. Hackley, Y.-M. Choi, J. Electrochem. Soc. 152 (2005) A1763, https://doi.org/10.1149/1.1979214.
[21] M. Wang, K. Liu, J. Yu, Q. Zhang, Y. Zhang, M. Valix, D.C.W. Tsang, Glob. Chall. 7 (2023) 2200237, https://doi.org/10.1002/gch2.202200237.
[22] R. Yu, C. Zhou, X. Zhou, J. Yang, J. Tang, Y. Zhang, Materials 17 (2024) 3883, https://doi.org/10.3390/ma17163883.
[23] H. Lee, Y.-T. Kim, S.-W. Lee, Energies 16 (6) (2023) 2759, https://doi.org/10.3390/en16062759.
[24] Y. Bai, L. Yu, I. Belharouak, J. Power Sources 592 (2024) 233954, https://doi.org/10.1016/j.jpowsour.2023.233954.
[25] Y. Zhao, Y. Kang, M. Fan, T. Li, J. Wozny, Y. Zhou, X. Wang, Y.-L. Chueh, Z. Liang, G. Zhou, J. Wang, N. Tavajohi, F. Kang, B. Li, Energy Storage Mater. 45 (2022) 1092, https://doi.org/10.1016/j.ensm.2021.11.005.
[26] J.A. Gilbert, I.A. Shkrob, D.P. Abraham, J. Electrochem. Soc. 164 (2017) A389, https://doi.org/10.1149/2.1111702jes.
[27] Y. Liu, H. Wen, Y. Chen, X. Yang, Y. Liu, B. Zhao, G. Jiang, Environ. Sci. & Technol. 60 (2026) 6589, https://doi.org/10.1021/acs.est.5c12432.
[28] M. Ullah, H. Shalchian, T. Younas, F. Vegliò, N.M. Ippolito, Process. Saf. Environ. Prot. 202 (2025) 107710, https://doi.org/10.1016/j.psep.2025.107710.
[29] M.S. Rana, A. Rahim, R. Hasan, M. Shahinuzzaman, A.N. Ahmed, M.S. Quddus, C. K. Roy, M. Hossain, M.S. Jamal, Nanoscale Adv. 8 (2026) 1423, https://doi.org/10.1039/d5na00957j.
[30] A. Sokhanpazhou, S.M. Masoudpanah, H. Nasrinpour, Results Eng. 28 (2025) 107971, https://doi.org/10.1016/j.rineng.2025.107971.
[31] M. Wang, Q. Tan, L. Liu, J. Li, ACS Sustain. Chem. Eng. 7 (2019) 12799, https://doi.org/10.1021/acssuschemeng.9b01546.
[32] K. Min, E. Cho, Phys. Chem. Chem. Phys. 20 (2018) 27115, https://doi.org/10.1039/C8CP04927K.
[33] H. Wang, Y. Huang, C. Huang, X. Wang, K. Wang, H. Chen, S. Liu, Y. Wu, K. Xu, W. Li, Electrochim. Acta 313 (2019) 423, https://doi.org/10.1016/j.electacta.2019.05.050.
[34] Y. Tzeng, C.-Y. Jhan, Y.-H. Wu, Nanomaterials 12 (3) (2022) 469, https://doi.org/10.3390/nano12030469.
[35] B. Xing, C. Zhang, Y. Cao, G. Huang, Q. Liu, C. Zhang, Z. Chen, G. Yi, L. Chen, J. Yu, Fuel Process. Technol. 172 (2018) 162, https://doi.org/10.1016/j.fuproc.2017.12.018.
[36] N.C. Gallego, C.I. Contescu, H.M. Meyer III, J.Y. Howe, R.A. Meisner, E.A. Payzant, M.J. Lance, S.Y. Yoon, M. Denlinger, D.L. Wood III, CARBON 72 (2014) 393, https://doi.org/10.1016/j.carbon.2014.02.031.
[37] T. Koita, Y. Imaizumi, A. Narita, Y. Takaya, Y. Kita, H. Akashi, T. Namihira, C. Tokoro, Waste Manag. 198 (2025) 46, https://doi.org/10.1016/j.wasman.2025.02.039.
[38] Y. Sawaki, N. Matsumoto, Y.M. Todorov, K. Abe, Method for manufacturing electrode active material, method for manufacturing secondary battery and secondary battery, WO2024048571A1, 2024; JP7766309B2, 2025; EP4583246B1, 2026.